

## Kinetics of Fe<sup>2+</sup>-Mg order-disorder in P<sub>2</sub>/c pigeonite

M. CHIARA DOMENEGHETTI,\* MICHELE ZEMA, AND VITTORIO TAZZOLI

Dipartimento di Scienze della Terra, Università di Pavia, Via Ferrata 1, 27100 Pavia, Italy

### ABSTRACT

The kinetics of the Fe-Mg intracrystalline exchange reaction in P<sub>2</sub>/c pigeonite (Wo<sub>10</sub>En<sub>47</sub>Fs<sub>43</sub>) free of exsolved augite, from the Paraná rhyodacite sample BTS308, was studied by single-crystal X-ray diffraction (XRD). Isothermal disordering annealing experiments, with oxygen fugacity controlled at the IW buffer, were performed on two crystals at 650, 700, 750, and 800 °C until the Fe-Mg exchange equilibrium was reached. The XRD data were collected from the two untreated crystals and after each annealing experiment. Structure refinements were carried out taking into account the recently discovered stronger preference of Mn for the M2 site compared to Fe<sup>2+</sup>. The linear regression of ln  $k_D^*$  vs. 1/T yielded the following equation:

$$\ln k_D^* = -2925(\pm 110)/T(K) + 0.574(\pm 0.111); (R^2 = 0.997)$$

The  $T_c$  values calculated using this equation were 566 (±6) and 571 (±6) °C for the two crystals. Analysis of the kinetic data was performed according to Mueller's model, which allowed retrieval of the disordering rate constants  $C_0K_{dis}^*$  for all four temperatures. The Arrhenius relation:

$$\ln K_{dis}^* = \ln K_0 - Q/(RT) = 20.45(\pm 1.91) - 25191 (\pm 1900)/T(K); (R^2 = 0.989)$$

yielded an activation energy of 50.03 (±3) kcal/mol for the Fe-Mg exchange process. Cooling time constants, calculated at the QMF buffer conditions of the host rock were, for the two crystals,  $\eta = 0.94 \times 10^{-1} \text{ K}^{-1}\text{year}^{-1}$  and  $\eta = 1.10 \times 10^{-1} \text{ K}^{-1}\text{year}^{-1}$ , and gave cooling rates on the order of 10 °C/h consistent with very fast lava cooling.

### INTRODUCTION

Pigeonite (Mg, Fe<sup>2+</sup>, Ca) (Mg, Fe<sup>2+</sup>) (Si<sub>2</sub>O<sub>6</sub>) is a Ca-poor clinopyroxene frequently occurring in terrestrial and extraterrestrial volcanic rocks. At high temperature, pigeonite is monoclinic C2/c but, on cooling, a displacive, reversible, and composition-dependent phase transition takes place with change of space group to P<sub>2</sub>/c (Prewitt et al. 1971; Brown et al. 1972; Sueno et al. 1984). In P<sub>2</sub>/c pigeonite, as well as in Pbc orthopyroxene and C2/c clinopyroxene, a non-convergent order-disorder process, involving the distribution of Fe<sup>2+</sup> and Mg between the M1 and M2 structural sites, occurs and can be described by the intracrystalline exchange reaction Fe<sup>2+</sup>(M1) + Mg(M2) ↔ Fe<sup>2+</sup>(M2) + Mg(M1). For orthopyroxene, the dependence on temperature and composition of both the equilibrium (Saxena and Ghose 1971; Molin et al. 1991; Yang and Ghose 1994; Stimpfl et al. 1999; Schlenz et al. 2001) and kinetic behaviors (Virgo and Hafner 1969; Besancon 1981; Anovitz et al. 1988; Saxena et al. 1987, 1989; Skogby 1992; Sykes-Nord and Molin 1993; Ganguly and Tazzoli 1994; Zema et al. 1999, 2003; Heinemann et al. 2000) of the Fe-Mg exchange reaction have been characterized, thus allowing this mineral to be used as a “geospeedometer” for retrieving the thermal history of terrestrial and extraterrestrial host rocks (Ganguly 1982; Ganguly et

al. 1994; Molin et al. 1994; Ganguly and Domeneghetti 1996; Kroll et al. 1997; Zema et al. 1997; Domeneghetti et al. 2000). For C2/c clinopyroxene, the equilibrium of Fe-Mg exchange has been studied in samples with different compositions and at different  $T$  enabling geothermometric applications (McCallister et al. 1976; Molin and Zanazzi 1991) while the kinetics has been characterized by ordering experiments using an augitic sample with composition ca. Wo<sub>43</sub>En<sub>46</sub>Fs<sub>11</sub> (Brizi et al. 2001). For P<sub>2</sub>/c pigeonite, the temperature dependence of the Fe-Mg order-disorder under equilibrium conditions has been studied by Pasqual et al. (2000) using two samples with different Mg/Fe ratios and Ca content. By linear regression of ln  $k_D^*$  vs. 1/T, Pasqual et al. (2000) obtained two geothermometric calibrations which allowed the closure temperature ( $T_c$ ) of the Fe-Mg order-disorder reaction in a pigeonite-bearing rock to be calculated. However, the lack of kinetic data prevented evaluation of the cooling history for the host rock.

To fill this gap, we carried out a series of kinetic experiments using the same pigeonite sample BTS308 studied by Pasqual et al. (2000), which has a suitable Fe/Fe + Mg composition and was shown to be free of exsolution products. Experimental annealing temperatures ranged from 650 to 800 °C, well below the transition temperature (from P<sub>2</sub>/c to C2/c) of between 875 and 925 °C found for this sample by Cámara et al. (2002). The degree of Fe-Mg order was measured by single-crystal X-ray diffraction (XRD) and the treatment of the kinetic data was performed on the

\* E-mail: domeneghetti@crystal.unipv.it

basis of Mueller's model (1967, 1969) as developed by Ganguly (1982). According to this model the Fe-Mg exchange reaction in pigeonite was treated, as in orthopyroxene, as a homogeneous chemical reaction following a second-order kinetic law.

Preliminary results of this study were presented by Domeneghetti et al. (2004). However in the present paper the treatment of the XRD data was slightly modified to take into account the behavior of Mn with temperature that Stimpfl (2005) recently observed in annealing experiments involving a donpeacorite ( $\text{Mn}_{0.54}\text{Ca}_{0.03}\text{Mg}_{1.43}\text{Si}_2\text{O}_6$ ) sample. The equilibrium behavior at temperatures ranging from 980 to 800 °C showed that Mn has a much stronger preference than  $\text{Fe}^{2+}$  for the M2 site. Thus, although the Mn content of the BTS308 pigeonite sample is low (0.029 apfu), a new M1 and M2 site distribution was obtained by taking into account the stronger preference for M2 of Mn compared to  $\text{Fe}^{2+}$ , instead of following the assumption so far adopted for clino- and orthopyroxenes, that Mn partitions between the two octahedral sites in the same way as  $\text{Fe}^{2+}$  (Hawthorne and Ito 1978).

## EXPERIMENTAL METHOD

### Samples

Two single pigeonite crystals with composition ca.  $\text{Wo}_{10}\text{En}_{47}\text{Fs}_{43}$  from the Paraná (Brazil) rhyodacite BTS308 (Secco et al. 1988) were used in this study. These samples, labeled BTS308 N.13 and BTS308 N.35 (sizes  $0.35 \times 0.19 \times 0.12$  mm and  $0.36 \times 0.31 \times 0.22$  mm, respectively), were selected after X-ray diffraction analyses and structure refinements for the similarity of their structural parameters and Mg- $\text{Fe}^{2+}$  order degree. In their microtextural study, Pasqual et al. (2000) showed that the BTS308 pigeonite sample does not contain exsolved augite lamellae. This was confirmed by analysis of single-crystal diffraction rocking profiles.

### Annealing experiments

Isothermal heating experiments were performed until equilibrium at 650 and 750 °C on crystal BTS308 N.13 and at 700 and 800 °C on crystal BTS308 N.35 in a vertical temperature-controlled furnace [ $\pm 3$  °C, Pt/(Pt-Rh) thermocouple]. Since crystal N.35 was lost after the 28 min annealing experiment at 800 °C, the equilibrium at this temperature was confirmed using crystal N.13 once it had reached equilibrium at 750 °C. For each annealing experiment the crystal was sealed into silica vials, after alternately washing with Ar flux and vacuuming, together with an iron-wüstite buffer to control the  $f_{\text{O}_2}$ . Inside the silica tubes the crystal and the buffer were put into two small, separate Pt crucibles to avoid contact between them. Heating experiments were quenched by dropping the tubes into cold water. The presence of both iron and wüstite, in a different ratio compared to that in the original powder, was verified at the end of each experiment by X-ray powder diffraction. The sequence and durations of the experiments are reported in Table 1.

### X-ray single-crystal diffraction

Intensity data were collected with a three-circle Bruker AXS SMART APEX diffractometer equipped with a CCD detector (graphite-monochromatized  $\text{MoK}\alpha$  radiation,  $\lambda = 0.71073$  Å, 40 kV, 25 mA), using the Bruker SMART set of programs. A total of 3360 frames (resolution  $512 \times 512$  pixels) were collected with four different goniometer settings using the  $\omega$ -scan mode (scan width:  $0.2^\circ \omega$ ; exposure time: 10 s/frame; detector-sample distance: 4.02 cm). Completeness of the measured data was achieved up to  $38^\circ \theta$ . The Bruker program SAINT+ was used for data reduction, including intensity integration and background and Lorentz-polarization corrections. The semi-empirical absorption correction of Blessing (1995), based on the determination of transmission factors for equivalent reflections, was applied using the program SADABS (Sheldrick 1996). The unit-cell parameters, obtained by a least-squares procedure which refines the position of about 900 reflections in the range  $12$ – $22^\circ \theta$ , are reported in Table 1.

### Electron microprobe analysis

Since crystal N.35 was lost and crystal N.13 was preserved for further studies, chemical analysis was performed on another BTS308 pigeonite crystal which, after X-ray data collection and structure refinement using the same procedure as for samples N.13 and N.35, showed very similar structural parameters. A Cameca-Camebax electron microprobe with a fine-focused beam (1  $\mu\text{m}$  diameter) operating in the wavelength-dispersive (WDS) mode was used. Operating conditions were 15 kV accelerating voltage and 25 nA beam current; counting times were 20 s for peaks and 20 s for backgrounds. The following synthetic end-member mineral standards were used: diopside for Mg, ferrosilite for Fe, wollastonite for Si and Ca, chromite for Cr, corundum for Al, and  $\text{MnTiO}_3$  for Mn and Ti. A natural albite sample (Amelia albite) was used for Na. X-ray counts were converted into oxide weight percentages using the PAP correction program. Analyses are precise to within 1% for major elements and 3–5% for minor elements. Only those spot analyses with oxide totals of  $100 \pm 1$ , total cation contents of  $4.000 \pm 0.005$  atoms on the basis of six oxygen atoms and charge balance  $3^{41}\text{Al} + \text{Na} - 3^{61}\text{Al} - 4\text{Ti} - 3\text{Cr} \leq |0.005|$  were selected and averaged. The chemical analysis is reported in Table 2. It appears to be very close to that obtained by Pasqual et al. (2000) from another BTS308 pigeonite crystal, thus confirming the compositional homogeneity of this sample.

### Structure refinement

Equivalent reflections were averaged and the resulting internal agreement factors  $R_{\text{int}}$  are reported in Table 1. The structure refinements, based on  $F_o^2$ , were carried out in space group  $P2_1/c$  using the program CRYSTALS (Betteridge et al. 2003) following the results of the leverage analysis performed on the same pigeonite sample by Merli et al. (2002). The atomic scattering curves were taken from the *International Tables for X-ray Crystallography* (Ibers and Hamilton 1974). Neutral vs. ionized scattering factors were refined for all sites that are not involved in chemical substitutions (Hawthorne et al. 1995). Structure factors were weighted according to Chebychev schemes (Carruthers and Watkin 1979). An isotropic extinction parameter  $x$  (Larson 1970) was refined. A residual electron-density maximum, located  $0.5$ – $0.6$  Å from the M2 site, was observed in the difference-Fourier map for crystals n.13 and n.35 before and after all the annealing experiments. The same feature had previously been observed by Cámara et al. (2002) in another BTS308 pigeonite crystal, and by Tribaudino and Nestola (2002) in two synthetic  $P2_1/c$

**TABLE 1A.** Unit-cell parameters and details of data collections and structure refinements for crystal N.35 before and after annealing at 700 °C

	<i>a</i> (Å)	<i>b</i> (Å)	<i>c</i> (Å)	$\beta$ (°)	<i>V</i> (Å <sup>3</sup> )	<i>I</i> <sub>tot</sub>	<i>I</i> <sub>ind</sub>	<i>R</i> <sub>int</sub> (%)	<i>R</i> <sub>all</sub> (%)	<i>R</i> <sub>w</sub> (%)	<i>S</i>	m.a.n. M1	m.a.n. M2	m.a.n. M1+M2
Untreated	9.7071(14)	8.9435(13)	5.2481(8)	108.483(4)	432.11(11)	8159	2237	1.82	3.40	4.53	1.023	15.08(4)	22.77(6)	37.85
10 min	9.7093(14)	8.9417(13)	5.2479(7)	108.507(3)	432.05(11)	8159	2248	1.86	4.25	4.38	1.020	15.17(4)	22.65(6)	37.82
20 min	9.7057(13)	8.9396(12)	5.2453(7)	108.478(3)	431.65(10)	8172	2241	1.98	4.25	4.44	0.997	15.25(4)	22.63(6)	37.88
30 min	9.7118(14)	8.9442(13)	5.2484(7)	108.496(3)	432.35(11)	8117	2243	1.84	4.30	4.32	1.003	15.30(4)	22.61(6)	37.91
50 min	9.7114(14)	8.9473(13)	5.2513(7)	108.475(3)	432.77(11)	8159	2238	1.99	4.20	4.26	1.005	15.37(4)	22.50(7)	37.87
90 min	9.7087(12)	8.9405(11)	5.2468(7)	108.496(3)	431.90(10)	8166	2247	2.02	4.20	4.04	0.989	15.49(4)	22.37(5)	37.86
180 min	9.7104(12)	8.9417(12)	5.2476(7)	108.479(3)	432.14(10)	8136	2238	1.89	4.13	4.68	0.968	15.57(4)	22.34(6)	37.91
300 min	9.7120(12)	8.9434(11)	5.2492(7)	108.479(3)	432.43(10)	8168	2239	1.89	4.12	4.21	0.996	15.58(4)	22.31(6)	37.90
600 min	9.7132(13)	8.9469(12)	5.2500(7)	108.484(3)	432.70(10)	8149	2241	2.05	4.31	4.35	1.031	15.55(4)	22.33(6)	37.88
1000 min	9.7096(14)	8.9421(13)	5.2464(7)	108.476(3)	432.04(11)	8126	2244	1.88	4.39	4.36	0.979	15.59(4)	22.31(7)	37.90

Note: Standard deviations are given in parentheses.

$R_{\text{int}} = \sum |F_o^2 - F_o^2(\text{mean})| / \sum |F_o^2|$ ;  $R_{\text{all}} = \sum ||F_o - |F_c|| / \sum |F_o|$ ;  $S = [\sum (w(F_o^2 - F_c^2)^2) / (n - p)]^{0.5}$ , where *n* is the number of reflections and *p* is the total number of parameters refined. *I*<sub>tot</sub> is the total number of reflections after merging identical reflections (redundancy of measurements was ca. 1.75); *I*<sub>ind</sub> is the number of independent reflections used for structure refinements; m.a.n. is the mean atomic number.

**TABLE 1B.** Unit-cell parameters and details of data collections and structure refinements for crystal N.35 and N.13 after annealing at 800 °C

	<i>a</i> (Å)	<i>b</i> (Å)	<i>c</i> (Å)	β (°)	<i>V</i> (Å <sup>3</sup> )	<i>I</i> <sub>tot</sub>	<i>I</i> <sub>ind</sub>	<i>R</i> <sub>int</sub> (%)	<i>R</i> <sub>all</sub> (%)	<i>R</i> <sub>w</sub> (%)	<i>S</i>	m.a.n. M1	m.a.n. M2	m.a.n. M1+M2
N.35 1.5 min	9.7069(12)	8.9427(11)	5.2470(7)	108.458(3)	432.04(10)	8167	2239	1.80	4.26	4.37	1.011	15.63(4)	22.24(6)	37.87
N.35 3.5 min	9.7088(13)	8.9429(12)	5.2473(7)	108.471(3)	432.13(10)	8134	2233	1.79	4.13	4.66	0.977	15.69(4)	22.22(6)	37.91
N.35 6 min	9.7094(12)	8.9457(11)	5.2478(7)	108.468(3)	432.34(10)	8136	2245	1.91	4.11	4.45	1.000	15.74(4)	22.19(6)	37.93
N.35 10 min	9.7113(13)	8.9455(12)	5.2504(7)	108.478(3)	432.60(10)	8148	2238	2.03	4.28	4.61	1.018	15.83(4)	22.07(6)	37.89
N.35 18 min	9.7134(12)	8.9482(10)	5.2485(6)	108.463(3)	432.71(10)	8125	2247	1.73	3.82	4.39	1.004	15.88(4)	22.03(6)	37.91
N.13 60 min	9.7075(12)	8.9444(9)	5.2461(6)	108.485(3)	432.01(15)	8323	2290	1.86	4.10	4.73	0.982	15.87(4)	21.99(6)	37.86

Note: Standard deviations are given in parentheses.

**TABLE 1C.** Unit-cell parameters and details of data collections and structure refinements for crystal N.13 before and after annealing at 650 °C

	<i>a</i> (Å)	<i>b</i> (Å)	<i>c</i> (Å)	β (°)	<i>V</i> (Å <sup>3</sup> )	<i>I</i> <sub>tot</sub>	<i>I</i> <sub>ind</sub>	<i>R</i> <sub>int</sub> (%)	<i>R</i> <sub>all</sub> (%)	<i>R</i> <sub>w</sub> (%)	<i>S</i>	m.a.n. M1	m.a.n. M2	m.a.n. M1+M2
Untreated	9.7060(13)	8.9400(12)	5.2460(7)	108.504(4)	431.67(10)	8335	2294	1.53	4.13	4.05	0.985	15.08(4)	22.79(6)	37.87
80 min	9.7096(13)	8.9413(12)	5.2473(6)	108.515(4)	431.97(10)	10713	2365	2.09	4.29	6.04	1.023	15.19(4)	22.74(6)	37.93
120 min	9.7084(12)	8.9414(11)	5.2476(6)	108.505(4)	431.97(10)	10771	2363	1.89	4.14	5.48	1.011	15.21(4)	22.70(8)	37.91
240 min	9.7086(12)	8.9421(11)	5.2473(7)	108.503(3)	432.00(10)	8376	2297	1.64	3.79	4.33	1.015	15.25(4)	22.63(6)	37.88
360 min	9.7074(17)	8.9415(16)	5.2468(10)	108.485(4)	431.92(14)	8378	2293	1.64	3.88	4.42	0.969	15.30(4)	22.59(6)	37.89
840 min	9.7083(14)	8.9419(12)	5.2481(7)	108.496(3)	432.06(10)	8348	2295	1.77	3.70	4.31	1.028	15.38(4)	22.49(5)	37.87
1680 min	9.7050(13)	8.9419(12)	5.2454(7)	108.485(3)	431.72(10)	8396	2302	1.67	3.66	4.27	1.017	15.40(4)	22.50(5)	37.90
3120 min	9.7096(14)	8.9413(12)	5.2470(7)	108.499(3)	431.99(10)	8364	2286	1.71	3.74	4.37	1.022	15.41(4)	22.46(5)	37.87
7440 min	9.7079(14)	8.9442(13)	5.2463(8)	108.485(3)	432.03(11)	8392	2285	1.52	3.43	4.20	1.018	15.39(4)	22.50(5)	37.88

Note: Standard deviations are given in parentheses.

**TABLE 1D.** Unit-cell parameters and details of data collections and structure refinements for crystal N.13 after annealing at 750 °C

	<i>a</i> (Å)	<i>b</i> (Å)	<i>c</i> (Å)	β (°)	<i>V</i> (Å <sup>3</sup> )	<i>I</i> <sub>tot</sub>	<i>I</i> <sub>ind</sub>	<i>R</i> <sub>int</sub> (%)	<i>R</i> <sub>all</sub> (%)	<i>R</i> <sub>w</sub> (%)	<i>S</i>	m.a.n. M1	m.a.n. M2	m.a.n. M1+M2
9 min	9.7071(12)	8.9425(11)	5.2463(7)	108.484(3)	431.91(10)	8108	2196	1.67	4.13	4.28	0.990	15.56(4)	22.35(6)	37.91
15 min	9.7100(12)	8.9425(11)	5.2470(6)	108.495(3)	432.07(10)	8137	2217	1.79	4.27	4.09	1.017	15.56(4)	22.31(6)	37.86
25 min	9.7086(12)	8.9436(11)	5.2464(7)	108.491(3)	432.03(10)	8151	2235	1.61	4.17	3.71	0.996	15.62(4)	22.25(6)	37.88
50 min	9.7100(14)	8.9462(13)	5.2480(7)	108.494(3)	432.34(11)	8167	2243	1.69	3.98	4.24	1.004	15.71(4)	22.19(6)	37.90
100 min	9.7103(11)	8.9444(10)	5.2490(6)	108.468(3)	432.41(10)	8200	2237	1.64	4.31	3.85	1.022	15.72(4)	22.21(5)	37.92
250 min	9.7109(13)	8.9437(12)	5.2477(7)	108.469(3)	432.29(10)	8137	2178	1.85	3.99	4.25	1.024	15.74(4)	22.17(5)	37.91

Note: standard deviations are given in parentheses.

clinopyroxene samples with compositions  $\text{Di}_{15}\text{En}_{85}$  and  $\text{Di}_{23}\text{En}_{77}$ . As suggested by these authors, this residual electron density is due to positional disorder of Ca at the M2 site. A split position M21, occupied by Ca, with the atomic coordinates of the residual (ca.  $x = 0.25$ ,  $y = 0.08$ ,  $z = 0.26$ ), was then introduced into the structure refinement. Anisotropic refinement performed for all atoms except M21 produced a slight improvement in the agreement factor with respect to the non-split model. When the refinement reached convergence, full-matrix least-squares with chemical constraints taken from the electron microprobe analysis (Table 2) and assuming  $1\sigma$  as error were carried out to obtain the site partitioning.

As mentioned above, M1 and M2 site partitioning was obtained taking into account the stronger preference of Mn for M2 compared to  $\text{Fe}^{2+}$  observed by Stimpfl (2005). However, instead of considering Mn totally ordered at the M2 site, as recommended by Stimpfl (2005), the following equation:

$$\left[ \frac{X_{\text{Mn}}^{\text{M2}}}{X_{\text{Mn}}^{\text{M1}}} \right] \left[ \frac{X_{\text{Fe}}^{\text{M1}}}{X_{\text{Fe}}^{\text{M2}}} \right] = k_{\text{D(Mn-Mg)}}/k_{\text{D(Fe}^{2+}\text{-Mg)}} = 2.447 \cdot e^{195/T(\text{K})} \cong 2.9 \quad (1)$$

was used as a restraint in the structure refinements to better approximate the actual distribution of Mn between M1 and M2 with temperature. This equation was calculated by comparing the calibration  $\ln k_{\text{D(Mn-Mg)}} = -2752/T(\text{K}) - 0.348$  obtained by Stimpfl (2005) for Mn-rich/Fe-free orthopyroxene with the calibration  $\ln k_{\text{D(Fe}^{2+}\text{-Mg)}} = -2557/T(\text{K}) - 0.547$  obtained by Stimpfl et al. (1999) for Fe-Mg orthopyroxenes, with low Mn contents, in the  $X_{\text{Fe}}$  range 0.19–0.75.

In addition to Equation 1, the following restraints were introduced into the refinement: (1) all structural sites were considered fully occupied; (2) Al was distributed between the TB and M1 sites and  $\text{Fe}^{3+}$ ,  $\text{Cr}^{3+}$ , and  $\text{Ti}^{4+}$  were considered fully ordered at the M1 site while Mg and  $\text{Fe}^{2+}$  were allowed to fractionate between the M1 and M2 sites; (3) Na was assumed to occupy the M2 site while Ca was distributed between M2 and M21 with  $X_{\text{Ca}}^{\text{M2}} + X_{\text{Ca}}^{\text{M21}} = X_{\text{Ca}}$ ; (4) charge balance in the isomorphous replacements was ensured by the equation  $X_{\text{Al}} + 2X_{\text{Ti}^{4+}} + X_{\text{Cr}^{3+}} = X_{\text{Na}} + X_{\text{Al}}^{\text{M1}}$ . The site populations as well as the values of the equilibrium distribution coefficients  $k_{\text{D}}^{\text{M1}}$  are reported in Table 3. The values of the conventional agreement indices  $R_1$  and  $R_{\text{all}}$ , as well as the goodness of fit ( $S$ ) are reported in Table 1 together with the mean atomic numbers (m.a.n.) at the M1 and M2 sites for the two untreated crystals n.13 and n.35 and for all the annealing experiments. The final atomic parameters are given in Table 5.<sup>1</sup>

**TABLE 2.** Electron microprobe analysis of the BTS308 pigeonite sample

Oxide (wt%)		Atoms per formula unit*
$\text{SiO}_2$	51.18(24)	Si 1.967(4)
$\text{Al}_2\text{O}_3$	0.71(3)	Al 0.032(2)
$\text{TiO}_2$	0.36(3)	Ti 0.010(1)
$\text{Cr}_2\text{O}_3$	0.01(2)	Cr –
FeO	26.46(29)	$\text{Fe}^{2+}$ 0.836(8)
		$\text{Fe}^{3+}$ 0.014(5)
MnO	0.90(8)	Mn 0.029(3)
MgO	16.02(9)	Mg 0.918(5)
CaO	4.65(7)	Ca 0.191(3)
NaO	0.04(2)	Na 0.003(1)
Sum	100.33	Sum 4.000

Note: Standard deviations are given in parentheses; average of 15 electron microprobe analyses.

\* Based on six O atoms.

## RESULTS AND DISCUSSION

As previously indicated, the cation distribution between M1 and M2 sites was obtained neither by partitioning Mn in the same way as  $\text{Fe}^{2+}$  (Hawthorne and Ito 1978) nor by considering it totally ordered at M2 (Stimpfl 2005), but in accordance with Equation 1. The calculation of atomic fractions  $X_{\text{Fe}^{2+}}^{\text{M1}}$  and  $X_{\text{Fe}^{2+}}^{\text{M2}}$

<sup>1</sup> Deposit item AM-05-027, Table 5. Deposit items are available two ways: For a paper copy contact the Business Office of the Mineralogical Society of America (see inside front cover of recent issue) for price information. For an electronic copy visit the MSA web site at <http://www.minsocam.org>, go to the American Mineralogist Contents, find the table of contents for the specific volume/issue wanted, and then click on the deposit link there.

**TABLE 3A.** Cation distribution, atomic fractions at M1 and M2 sites, and  $k_D^*$  values for crystal N.35 before and after annealing at 700 °C

	Untreated	10 min	20 min	30 min	50 min	90 min	180 min	300 min	600 min	1000 min
TB site										
Si	1.9681	1.9681	1.9680	1.9680	1.9680	1.9681	1.9679	1.9680	1.9680	1.9680
Al	0.0319	0.0319	0.0320	0.0320	0.0320	0.0319	0.0321	0.0320	0.0320	0.0320
M1 site										
Mg	0.7764(20)	0.7705(30)	0.7650(30)	0.7613(30)	0.7565(30)	0.7477(20)	0.7422(30)	0.7409(20)	0.7435(30)	0.7402(30)
Fe	0.1960(30)	0.2019(30)	0.2072(30)	0.2107(30)	0.2155(30)	0.2243(30)	0.2294(30)	0.2307(30)	0.2283(30)	0.2314(30)
Fe <sup>3+</sup>	0.0147	0.0146	0.0148	0.0149	0.0148	0.0147	0.0151	0.0150	0.0148	0.0150
Al	–	–	–	–	–	–	–	–	–	–
Cr	–	–	–	–	–	–	–	–	–	–
Ti	0.0101	0.0102	0.0101	0.0100	0.0101	0.0101	0.0100	0.0100	0.0101	0.0100
Mn	0.0027(2)	0.0028(4)	0.0030(2)	0.0030(4)	0.0031(5)	0.0032(4)	0.0033(3)	0.0034(3)	0.0033(1)	0.0034(4)
M2 site										
Mg	0.1437(30)	0.1519(30)	0.1539(30)	0.1551(30)	0.1628(30)	0.1723(30)	0.1747(30)	0.1764(30)	0.1750(30)	0.1769(30)
Fe	0.6362(40)	0.6279(40)	0.6259(40)	0.6248(40)	0.6172(50)	0.6079(40)	0.6061(40)	0.6041(40)	0.6051(30)	0.6035(40)
Ca	0.1912	0.1915	0.1913	0.1912	0.1913	0.1913	0.1907	0.1909	0.1913	0.1910
Mn	0.0259(20)	0.0256(30)	0.0259(20)	0.0261(40)	0.0256(40)	0.0255(30)	0.0255(20)	0.0255(20)	0.0255(30)	0.0256(30)
Na	0.0030	0.0031	0.0030	0.0029	0.0030	0.0030	0.0030	0.0030	0.0030	0.0030
$X_{Fe^+}^{M1}$	0.2038	0.2099	0.2155	0.2192	0.2242	0.2333	0.2387	0.2401	0.2375	0.2408
$X_{Fe^+}^{M2}$	0.8217	0.8114	0.8090	0.8076	0.7979	0.7861	0.7833	0.7811	0.7828	0.7805
$k_D^*$	0.0555(18)	0.0618(20)	0.0649(20)	0.0669(21)	0.0732(22)	0.0828(24)	0.0867(25)	0.0885(25)	0.0864(25)	0.0892(25)
$\ln k_D^*$	-2.8914	-2.7838	-2.7349	-2.7045	-2.6145	-2.4913	-2.4453	-2.3980	-2.4488	-2.4169

Note: Standard deviations are given in parentheses;

$$X_{Fe^+}^{M1} = (Fe + Mn)_{M1} / (Fe + Mn + Mg)_{M1}; X_{Fe^+}^{M2} = (Fe + Mn)_{M2} / (Fe + Mn + Mg)_{M2}; k_D^* = X_{Fe^+}^{M1} [1 - X_{Fe^+}^{M2}] / X_{Fe^+}^{M2} [1 - X_{Fe^+}^{M1}].$$

**TABLE 3B.** Cation distribution, atomic fractions at M1 and M2 sites, and  $k_D^*$  values for crystals N.35 and N.13 after annealing at 800 °C

	1.5 min	3.5 min	6 min	10 min	18 min	60 min†
TB site						
Si	1.9681	1.9679	1.9679	1.9680	1.9679	1.9681
Al	0.0319	0.0321	0.0321	0.0320	0.0321	0.0319
M1 site						
Mg	0.7374(30)	0.7330(30)	0.7296(30)	0.7236(30)	0.7194(30)	0.7206(30)
Fe	0.2344(30)	0.2385(30)	0.2418(30)	0.2478(30)	0.2518(30)	0.2508(30)
Fe <sup>3+</sup>	0.0146	0.0150	0.0150	0.0149	0.0149	0.0148
Al	–	–	–	–	–	–
Cr	–	–	–	–	–	–
Ti	0.0101	0.0100	0.0100	0.0100	0.0100	0.0101
Mn	0.0034(4)	0.0035(4)	0.0036(3)	0.0037(4)	0.0038(3)	0.0037(3)
M2 site						
Mg	0.1816(30)	0.1833(30)	0.1854(30)	0.1940(30)	0.1967(30)	0.1994(30)
Fe	0.5984(40)	0.5972(40)	0.5952(40)	0.5868(40)	0.5843(30)	0.5817(30)
Ca	0.1915	0.1910	0.1909	0.1910	0.1908	0.1910
Mn	0.0254(30)	0.0255(30)	0.0256(20)	0.0252(20)	0.0253(20)	0.0249(20)
Na	0.0030	0.0029	0.0029	0.0030	0.0029	0.0030
$X_{Fe^+}^{M1}$	0.2438	0.2482	0.2517	0.2579	0.2622	0.2610
$X_{Fe^+}^{M2}$	0.7745	0.7726	0.7700	0.7593	0.7560	0.7526
$k_D^*$	0.0939(26)	0.0972(27)	0.1004(28)	0.1102(30)	0.1146(31)	0.1161(26)
$\ln k_D^*$	-2.3655	-2.3310	-2.2986	-2.2054	-2.1663	-2.1533

Note: Standard deviations are given in parentheses.

† Performed on crystal N.13.

and of distribution coefficients  $k_D^*$  was carried out by considering the exchange of both Fe<sup>2+</sup> and Mn (denoted collectively as Fe<sup>\*</sup>) with Mg. The linear regression of  $\ln k_D^*$  vs.  $1/T$  for the four temperatures yielded the following equation:

$$\ln k_D^* = -2925(\pm 110)/T(K) + 0.574(\pm 111); (R^2 = 0.997) \quad (2)$$

The regression straight line reported in Figure 1 is in good agreement with that obtained by Pasqual et al. (2000) for another crystal from the same pigeonite sample (BTS308). The slightly more disordered Fe<sup>\*</sup>/Mg distribution recorded for that crystal at each temperature was already evident in the untreated crystal and was not a consequence of the different partitioning procedures employed in the two studies.

A comparison of  $k_D$  values for untreated crystal BTS308 N.13 was carried out by calculating  $k_D$  both from site partitioning obtained by disordering Mn in the same way as Fe<sup>2+</sup> and from that obtained by totally ordering Mn at M2. The calculated values were 0.0548(13) and 0.0567(16), respectively, very close to the observed value of 0.0545(15) (see Table 3c), thus confirming that, for this pigeonite composition, the different partitioning methods do not affect the  $k_D$  values as previously observed by Stimpfl (2005) for Mn-poor, Fe-rich ( $X_{Fe} = 0.19$ – $0.75$ ) orthopyroxenes.

The different order-disorder behavior of Mn compared to Fe<sup>2+</sup> implies treatment of the kinetic data that models an exchange reaction involving more than two cations. However, since in BTS308 pigeonite the variations in  $X_{Mn}^{M2}$  during the annealing experiments are all within the e.s.d.'s (see Table 3), Mueller's approach can still

**TABLE 3C.** Cation distribution, atomic fractions at M1 and M2 sites, and  $k_D^+$  values for crystal N.13 before and after annealing at 650 °C

	Untreated	80 min	120 min	240 min	360 min	840 min	1680 min	3120 min	7440 min
TB site									
Si	1.9680	1.9679	1.9680	1.9680	1.9680	1.9680	1.9679	1.9680	1.9680
Al	0.0320	0.0321	0.0320	0.0320	0.0320	0.0320	0.0321	0.0320	0.0320
M1 site									
Mg	0.7772(20)	0.7688(30)	0.7679(30)	0.7647(20)	0.7611(30)	0.7555(20)	0.7537(20)	0.7534(20)	0.7550(20)
Fe	0.1952(30)	0.2033(30)	0.2043(30)	0.2074(30)	0.2110(30)	0.2165(30)	0.2182(30)	0.2186(30)	0.2170(30)
Fe <sup>3+</sup>	0.0148	0.0150	0.0149	0.0148	0.0148	0.0147	0.0149	0.0148	0.0148
Al	–	–	–	–	–	–	–	–	–
Cr	–	–	–	–	–	–	–	–	–
Ti	0.0101	0.0100	0.0100	0.0101	0.0101	0.0101	0.0100	0.0101	0.0101
Mn	0.0027(2)	0.0029(4)	0.0029(2)	0.0029(3)	0.0030(2)	0.0031(3)	0.0031(3)	0.0031(2)	0.0031(3)
M2 site									
Mg	0.1420(30)	0.1463(40)	0.1484(30)	0.1537(30)	0.1570(30)	0.1638(30)	0.1633(30)	0.1659(30)	0.1634(30)
Fe	0.6379(30)	0.6341(40)	0.6316(40)	0.6267(40)	0.6232(30)	0.6168(30)	0.6173(40)	0.6145(30)	0.6171(30)
Ca	0.1911	0.1905	0.1909	0.1907	0.1910	0.1908	0.1907	0.1909	0.1908
Mn	0.0260(20)	0.0262(10)	0.0261(20)	0.0258(20)	0.0258(20)	0.0256(20)	0.0258(20)	0.0256(20)	0.0257(20)
Na	0.0030	0.0029	0.0029	0.0030	0.0030	0.0030	0.0029	0.0030	0.0030
$X_{Fe^*}^{M1}$	0.2030	0.2115	0.2125	0.2157	0.2195	0.2252	0.2270	0.2274	0.2257
$X_{Fe^*}^{M2}$	0.8238	0.8186	0.8159	0.8094	0.8052	0.7968	0.7975	0.7942	0.7973
$k_D^+$	0.0545(15)	0.0594(19)	0.0609(20)	0.0648(20)	0.0680(18)	0.0741(19)	0.0746(22)	0.0763(19)	0.0741(19)
$\ln k_D^+$	-2.9095	-2.8235	-2.7985	-2.7364	-2.6882	-2.6023	-2.5956	-2.5731	-2.6023

Note: Standard deviations are given in parentheses.

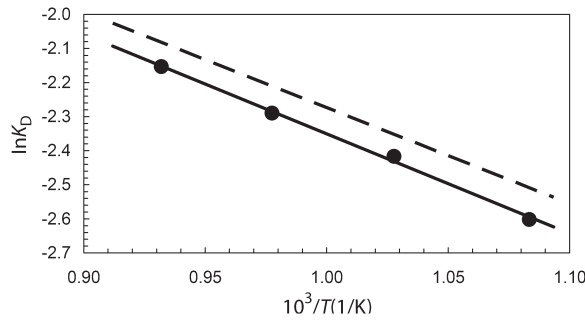


**FIGURE 1.** A  $\ln k_D^+$  vs.  $1/T(K)$  plot for the BTS308 pigeonite sample. The vertical size of the symbols exceeds the uncertainties in  $\ln k_D^+$ . The dashed line is the calibration by Pasqual et al. (2000).

be adopted with the advantage of providing kinetic results that can be compared with those obtained to date for the orthopyroxenes. Therefore Mueller's (1969) equation was used as follows:

$$-C_0 K_{dis}^+ \Delta t = \frac{1}{(b^2 - 4ac)^{1/2}} \ln \left[ \frac{(b^2 - 4ac)^{1/2} - (2aX_{Fe^*}^{M2} + b)}{(b^2 - 4ac)^{1/2} + (2aX_{Fe^*}^{M2} + b)} \right]_{X_{Fe^*}^{M2}(0)}^{X_{Fe^*}^{M2}(t)} \quad (3)$$

where  $C_0 = C_{M1} + C_{M2}$  is the total number of sites per unit volume involved in the exchange process that is usually included in the disordering rate constant  $K_{dis}^+$ ;  $a$ ,  $b$ , and  $c$  are coefficients which depend on the composition of the crystal and on the equilibrium distribution coefficient (see Table 3);  $X_{Fe^*}^{M2}$  is the atomic fraction used to define the Fe\*-Mg degree of order of the crystals.

The calculation of the disordering rate constants at the four temperatures was performed by plotting the term  $L$ :

$$L = \ln \left[ \frac{(b^2 - 4ac)^{1/2} - (2aX_{Fe^*}^{M2} + b)}{(b^2 - 4ac)^{1/2} + (2aX_{Fe^*}^{M2} + b)} \right]_{X_{Fe^*}^{M2}(0)}^{X_{Fe^*}^{M2}(t)} \quad (4)$$

**TABLE 4.** Disordering rate constants

$T$ (°C)	$C_0 K_{dis}^+$ (min <sup>-1</sup> )
650	$9.24 \times 10^{-4}$
700	$5.10 \times 10^{-3}$
750	$1.78 \times 10^{-2}$
800	$4.12 \times 10^{-2}$

i.e., the logarithmic term of Equation 2 vs.  $\Delta t$ . The slope of the resulting straight line yielded the values of the disordering rate constants  $C_0 K_{dis}^+$ ; these are reported in Table 4 while the variation of  $X_{Fe^*}^{M2}$  with annealing time at the various temperature is shown in Figure 2. As can be seen, there is a close fit between the theoretical curves calculated using the  $C_0 K_{dis}^+$  values in Mueller's equation and the experimental points, thus indicating a second-order kinetic law for the Fe-Mg exchange reaction and a high reliability for the measured ordering states. The values of the kinetic constants at 700, 750, and 800 °C appear to be higher than those obtained at the same temperatures by Brizi et al. (2001), who applied Mueller's method to an augitic clinopyroxene. However, this is consistent with the higher Fe content of the BTS308 pigeonite sample compared to augite ( $X_{Fe^*} = 0.49$  vs.  $X_{Fe^*} = 0.15$ ).

The Arrhenius relation:

$$\ln K_{dis}^+ = \ln K_0 - Q/(RT) = 20.45(\pm 1.91) - 25191 (\pm 1900)/T; \quad (R^2 = 0.989) \quad (5)$$

plotted in Figure 3 yielded an activation energy of 50.03(± 3.0) kcal/mol. This value is very close to that of 47.8 kcal/mol obtained by Brizi et al. (2001) from ordering experiments involving augite. In terms of the activation energy for the Fe-Mg exchange reaction in orthopyroxene, the value obtained in this study for pigeonite is significantly lower than both the average value of 62.8(± 2.2) kcal/mol obtained by Ganguly and Tazzoli (1994) from selected disordering data taken from the literature and the values of about 70 and 78 kcal/mol very recently obtained by

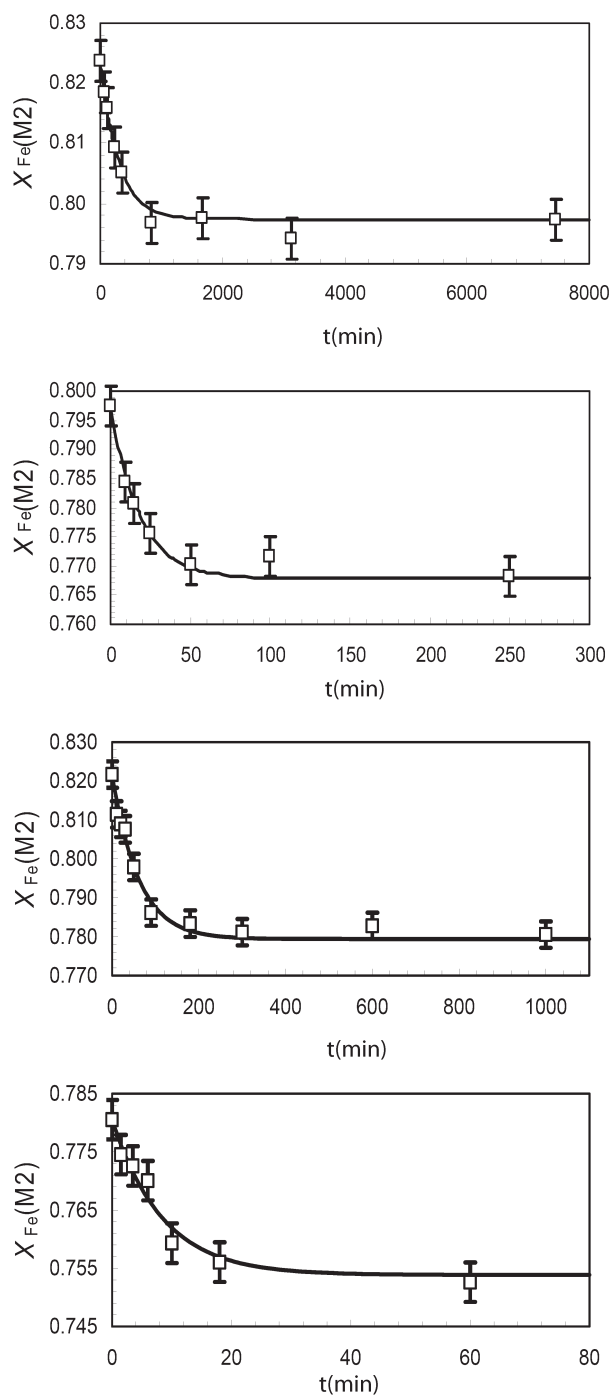


**FIGURE 2.** Experimental points superimposed on the theoretical curves calculated by Mueller's equation. From top to bottom: annealing at 650, 700, 750, and 800 °C.

Stimpfl et al. (pers. comm.) from ordering experiments on two orthopyroxenes with composition  $\text{Fs}_{30}$  and  $\text{Fs}_{17}$  respectively, according to the data of Ganguly and Stimpfl (2000).

The calibration  $\ln k_D^*$  vs.  $1/T$  (Eq. 2) was used to calculate the closure temperature for pigeonite sample BTS308. The  $T_c$  values

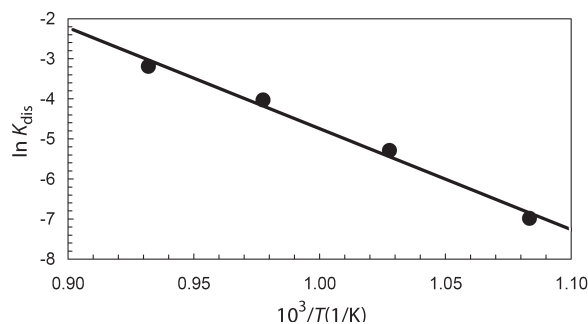


**FIGURE 3.** Arrhenius plot  $\ln K_{\text{dis}}^* = \ln K_0 - Q/(RT)$  which yields an activation energy of 50.03 kcal/mol for the Fe-Mg exchange process for the BTS308 pigeonite sample. The vertical size of the symbols exceeds the uncertainties in  $\ln K_{\text{dis}}^*$ . Dashed line: Arrhenius plot obtained by Brizi et al. (2001) for a  $\text{Wo}_{43}\text{En}_{46}\text{Fs}_{11}$  augite; dotted line: Arrhenius plot calculated for an orthopyroxene of composition  $X_{\text{Fe}} = 0.5$  using the equation of Ganguly and Tazzoli (1994).

for BTS308 crystals N.13 and N.35 were  $566(\pm 6)$  and  $571(\pm 6)$  °C, respectively. The cooling rate was calculated by shifting the kinetic constants, experimentally obtained with IW buffer, to the  $f_{\text{O}_2}$  conditions of the host rock. The  $f_{\text{O}_2}$  conditions of the Paraná rhyodacites, obtained from petrographic data (Bellieni et al. 1986), correspond to those controlled by a QMF buffer (calculated at 1 bar). Assuming, on the basis of the expected dependence of point-defect concentration on  $f_{\text{O}_2}$ , that the disordering rate constant is expected to increase with  $(f_{\text{O}_2})^{-1/6}$  (Nakamura and Schmalzried 1984; Ganguly and Domeneghetti 1996), the rate constants obtained at 650, 700, 750, and 800 °C with IW buffer were recalculated for the same temperatures as follows:

$$K_{\text{dis}}^+(\text{QMF})/K_{\text{dis}}^+(\text{IW}) = [f_{\text{O}_2}(\text{QMF})/f_{\text{O}_2}(\text{IW})]^{1/6} \quad (6)$$

The equilibrium data from Equation 2 and the recalculated kinetic data were used with the CRATE program (Ganguly, pers. comm.) to calculate the cooling time constants, according to the kinetic formulation discussed in Ganguly (1982). The cooling model was assumed to follow an asymptotic law ( $1/T = 1/T_0 + \eta t$  where  $\eta$  is the cooling time constant). The cooling time constants were  $\eta = 0.94 \times 10^{-1} \text{ K}^{-1}\text{year}^{-1}$  for crystal N.13 and  $\eta = 1.10 \times 10^{-1} \text{ K}^{-1}\text{year}^{-1}$  for crystal N.35. The resulting cooling rates  $r$  at the closure temperatures of 566 and 571 °C provided by the formula  $r = \eta \times T_c^2$  were on the order of 10 °C/h for both crystals. This high cooling rate for pigeonite BTS308, which comes from a rhyodacite lava flow in the Paraná basin, is in agreement with those obtained in the  $T_c$  range of 513–600 °C for augite samples from the middle of an andesitic lava flow on Salina Island in the Aeolian Islands (Molin and Zanazzi 1991).

The slightly higher disordering rate constants and activation energy data (within the e.s.d. values) for crystals N.13 and N.35, calculated on the basis of site partitioning in which Mn was disordered in the same way as  $\text{Fe}^{2+}$ , translate to a very small decrease in the cooling time constants (from  $\eta = 0.94 \times 10^{-1} \text{ K}^{-1}\text{year}^{-1}$  to  $\eta = 0.75 \times 10^{-1} \text{ K}^{-1}\text{year}^{-1}$  for crystal N.13 and from

$\eta = 1.10 \times 10^{-1} \text{ K}^{-1}\text{year}^{-1}$  to  $\eta = 0.89 \times 10^{-1} \text{ K}^{-1}\text{year}^{-1}$  for crystal N.35). Calculation of the cooling time constant carried out for comparison on untreated crystal N.13 from the site partitioning obtained by totally ordering Mn at M2 yielded a value of  $\eta = 1.28 \times 10^{-1} \text{ K}^{-1}\text{year}^{-1}$ , which corresponds to a cooling rate of ca.  $10^\circ/\text{h}$ , at  $T_c = 576^\circ\text{C}$ , without the change in the cooling rate evidenced by Stimpfl (2005) for low-Fe orthopyroxenes.

In the light of the results of this study, the following conclusions can be drawn: (1) for the composition of BTS308 pigeonite, the different site partitioning methods only have a slight effect on  $k_D$  values, as previously observed by Stimpfl (2005) for Mn-poor, Fe-rich orthopyroxenes, and on the kinetic constants; (2) the activation of the Fe-Mg intracrystalline exchange reaction in  $P2_1/c$  pigeonite and in  $C2/c$  augite requires the same energy; this is lower than in orthopyroxene and, as in orthopyroxene (Zema et al. 2003), it is not affected by the Ca content; (3) further kinetic studies are required on augite and pigeonite to better constrain the dependence of the kinetic constants and of the preexponential factor on  $X_{\text{Fe}}$ . This would allow correct evaluation of the cooling time constants and these clinopyroxenes could then be used as geospeedometers for retrieving the cooling history of their host rocks.

#### ACKNOWLEDGMENTS

This study was supported by the Italian project Cofin 2001 "Structural evolution and phase transitions in minerals as a function of temperature, pressure and composition". We are particularly grateful to R. Carampin for performing the electron microprobe analyses at the University of Padova. M. Stimpfl and G.M. Molin are acknowledged for their thorough reviews of the manuscript.

#### REFERENCES CITED

- Anovitz, L.M., Essene, E.J., and Dunham, W.R. (1988) Order-disorder experiments on orthopyroxenes: implications for the orthopyroxene geospeedometer. *American Mineralogist*, 73, 1060–1073.
- Belliemi, G., Comin-Chiaromonte, P., Marques, L.S., Melfi, A.J., Nardy, A.J.R., Papatrechas, C., Piccirillo, E.M., Roisenberg, A., and Stolfa, D. (1986) Petrogenetic aspects of acid and basaltic lavas from the Paraná Plateau (Brasil): Geological, mineralogical and petrochemical relationships. *Journal of Petrology*, 27, 915–944.
- Besancon, J.R. (1981) Rate of cation ordering in orthopyroxenes. *American Mineralogist*, 66, 965–973.
- Betteridge, P.W., Carruthers, J.R., Cooper, R.I., Prout, K., and Watkin, D.J. (2003) CRYSTALS version 12: software for guided crystal structure analysis. *Journal of Applied Crystallography*, 36, 1487.
- Blessing, R.H. (1995) An empirical correction for absorption anisotropy. *Acta Crystallographica*, A51, 33–38.
- Brizi, E., Molin, G.M., Zanazzi, P.F., and Merli, M. (2001) Ordering kinetics of Mg-Fe<sup>2+</sup> exchange in a Wo<sub>43</sub>En<sub>46</sub>Fs<sub>11</sub> augite. *American Mineralogist*, 86, 271–278.
- Brown, G.E., Prewitt, C.T., Papike, J.J., and Sueno, S. (1972) A comparison of the structure of low and high pigeonite. *Journal of Geophysical Research*, 77, 5778–5789.
- Cámara, F., Carpenter, M.A., Domeneghetti, M.C., and Tazzoli, V. (2002) Non-convergent ordering and displacive phase transition in pigeonite: in situ HT XRD study. *Physics and Chemistry of Minerals*, 29, 331–340.
- Carruthers, J.R. and Watkin, D.J. (1979) Chebyshev weighting. *Acta Crystallographica*, A35, 698–699.
- Domeneghetti, M.C., Molin, G.M., Triscari, M., and Zema, M. (2000) Orthopyroxene as a geospeedometer: thermal history of Kapoeta, Old Homestead 001 and Hughes 002 howardites. *Meteoritics and Planetary Science*, 35, 347–354.
- Domeneghetti, M.C., Zema, M., Schwartz, J.M., and Tazzoli, V. (2004) Kinetics of Fe<sup>2+</sup>-Mg order-disorder in  $P2_1/c$  pigeonite: implications for cooling rates calculations. *Lunar and Planetary Science XXXV*, Abstracts, 1145.
- Ganguly, J. (1982) Mg-Fe order-disorder in ferromagnesian silicates II. In S.K. Saxena, Ed., *Thermodynamics: Kinetics and Geological Applications*. Advances in Physical Geochemistry, 2, 58–99. Springer, Berlin.
- Ganguly, J. and Domeneghetti, M.C. (1996) Cation ordering of orthopyroxenes from the Skaergaard intrusion: implications for the subsolidus cooling rates and permeabilities. *Contributions to Mineralogy and Petrology*, 122, 359–367.
- Ganguly, J. and Stimpfl, M. (2000) Cation ordering in orthopyroxenes from two stony-iron meteorites: implications for cooling rates and metal-silicate mixing. *Geochimica et Cosmochimica Acta*, 64, 1291–1297.
- Ganguly, J. and Tazzoli, V. (1994) Fe<sup>2+</sup>-Mg interdiffusion in orthopyroxene: Retrieval from data on intracrystalline exchange reaction. *American Mineralogist*, 79, 930–937.
- Ganguly, J., Yang, H., and Ghose, S. (1994) Thermal history of mesosiderites: quantitative constraints from compositional zoning and Fe-Mg ordering in orthopyroxenes. *Geochimica et Cosmochimica Acta*, 58, 2711–2723.
- Hawthorne, F.C. and Ito, J. (1978) Refinement of the crystal structure of (Mg<sub>0.776</sub>Co<sub>0.224</sub>)SiO<sub>3</sub>. *Acta Crystallographica*, B34, 891–893.
- Hawthorne, F.C., Ungaretti, L., and Oberti, R. (1995) Site populations in minerals: terminology and presentation of results of crystal-structure refinement. *Canadian Mineralogist*, 33, 907–911.
- Heinemann, R., Kroll, H., Langenhorst, F., and Lueder, T. (2000) Time and temperature variation of the intracrystalline Fe<sup>2+</sup>-Mg fractionation in Johnstown meteoritic orthopyroxene. *European Journal of Mineralogy*, 12, 163–176.
- Ibers, J.A. and Hamilton, W.C., Eds. (1974) *International Tables for X-ray Crystallography*, vol. 4, pp. 99–101. Kynoch Press, Birmingham, U.K.
- Kroll, H., Lueder, T., Schlenz, H., Kirfel, A., and Vad, T. (1997) The Fe<sup>2+</sup>, Mg distribution in orthopyroxene: a critical assessment of its potential as a geospeedometer. *European Journal of Mineralogy*, 9, 705–733.
- Larson, A.C. (1970) The inclusion of secondary extinction in least-squares refinement of crystal structures. In F.R. Ahmed, S.R. Hall, and C.P. Huber, Eds., *Crystallographic Computing*, 291–294. Munksgaard, Copenhagen.
- McCallister, R.H., Finger, L.W., and Ohashi, Y. (1976) Intracrystalline Fe<sup>2+</sup>-Mg equilibria in three natural Ca-rich clinopyroxenes. *American Mineralogist*, 61, 671–676.
- Merli, M., Cámara, F., Domeneghetti, M.C., and Tazzoli, V. (2002) Leverage analysis of X-ray single crystal diffraction data from orthopyroxene and pigeonite. *European Journal of Mineralogy*, 14, 773–784.
- Molin, G.M. and Zanazzi, P.F. (1991) Intracrystalline Fe<sup>2+</sup>-Mg ordering in augite: experimental study and geothermometric applications. *European Journal of Mineralogy*, 3, 863–875.
- Molin, G.M., Saxena, S.K., and Brizi, E. (1991) Iron-magnesium order-disorder in an orthopyroxene crystal from the Johnstown meteorite. *Earth and Planetary Science Letters*, 105, 260–265.
- Molin, G.M., Domeneghetti, M.C., Salviulo, G., Stimpfl, M., and Tribaudino, M. (1994) Antarctic FRO90011 lodranite: cooling history from pyroxene crystal chemistry and microstructure. *Earth and Planetary Science Letters*, 128, 479–487.
- Mueller, R.F. (1967) Model for order-disorder kinetics in certain quasi-binary crystals of continuously variable composition. *Journal of Physics and Chemistry of Solids*, 28, 2239–2243.
- — — (1969) Kinetics and thermodynamics of intracrystalline distribution. *Mineralogical Society American Special Paper*, 2, 83–93.
- Nakamura, A. and Schmalzried, H. (1984) On the Fe<sup>2+</sup>-Mg<sup>2+</sup> interdiffusion in olivine (II). *Berichte Der Bunsen-Gesellschaft-Physical Chemistry Chemical Physics*, 88, 140–145.
- Pasqual, D., Molin, G., and Tribaudino, M. (2000) Single-crystal thermometric calibration of Fe-Mg order-disorder in pigeonites. *American Mineralogist*, 85, 953–962.
- Prewitt, C.T., Brown, G.E., and Papike, J.J. (1971) Apollo 12 clinopyroxenes. High-temperature X-ray diffraction studies. *Geochimica et Cosmochimica Acta Supplement*, 2, 1, 59–68.
- Saxena, S.K. and Ghose, S. (1971) Mg<sup>2+</sup>-Fe<sup>2+</sup> order-disorder and the thermodynamics of the orthopyroxene crystalline solution. *American Mineralogist*, 56, 532–559.
- Saxena, S.K., Tazzoli, V., and Domeneghetti, M.C. (1987) Kinetics of the Fe<sup>2+</sup>-Mg distribution in aluminous orthopyroxenes. *Physics and Chemistry of Minerals*, 15, 140–147.
- Saxena, S.K., Domeneghetti, M.C., Molin, G.M., and Tazzoli, V. (1989) X-ray diffraction study of Fe<sup>2+</sup>-Mg order-disorder in orthopyroxene. Some kinetic results. *Physics and Chemistry of Minerals*, 16, 421–427.
- Schlenz, H., Kroll, H., and Phillips, M.W. (2001) Isothermal annealing and continuous cooling experiments on synthetic orthopyroxenes: temperature and time evolution of the Fe,Mg distribution. *European Journal of Mineralogy*, 13, 715–726.
- Secco, L., Carbonin, S., Dal Negro, A., Mellini, M., and Piccirillo, E.M. (1988) Crystal chemistry of pyroxenes from basalts and rhodacites of the Paraná basin (Brazil). In E.M. Piccirillo and A.J. Melfi, Eds., *The Mesozoic Flood of the Paraná Basin: Petrogenetic and Geophysical Aspects*, p. 51–72. São Paulo University, Brazil.
- Sheldrick, G.M. (1996) SADABS. Institut für Anorganische Chemie der Universität, Göttingen, Germany.
- Skogby, H. (1992) Order-disorder kinetics in orthopyroxenes of ophiolite origin. *Contributions to Mineralogy and Petrology*, 109, 471–478.
- Stimpfl, M. (2005) The Mn, Mg-intracrystalline exchange reaction in donpeacorite (Mn<sub>0.54</sub>Ca<sub>0.03</sub>Mg<sub>1.47</sub>Si<sub>2</sub>O<sub>6</sub>) and its relation to the fractionation behavior of Mn in Fe, Mg-orthopyroxene. *American Mineralogist*, 90, 155–161.

- Stimpfl, M., Ganguly, J., and Molin, G.M. (1999) Fe<sup>2+</sup>-Mg order-disorder in orthopyroxene: equilibrium fractionation between the octahedral sites and thermodynamic analysis. *Contributions to Mineralogy and Petrology*, 136, 297–309.
- Sueno, S., Kimata, M., and Prewitt, C.T. (1984) The crystal structure of high clinoferrosilite. *American Mineralogist*, 69, 264–269.
- Sykes-Nord, J.A. and Molin, G.M. (1993) Mg-Fe order-disorder reaction in Fe-rich orthopyroxene: structural variation and kinetics. *American Mineralogist*, 78, 921–931.
- Tribaudino, M. and Nestola, F. (2002) Average and local structure in *P2<sub>1</sub>/c* clinopyroxenes along the join diopside-enstatite (CaMgSi<sub>2</sub>O<sub>6</sub>-Mg<sub>2</sub>Si<sub>2</sub>O<sub>6</sub>). *European Journal of Mineralogy*, 14, 549–555.
- Virgo, D. and Hafner, S.S. (1969) Fe<sup>2+</sup>-Mg disorder in heated orthopyroxenes. *Mineralogical Society of America, Special Paper*, 2, 67–81.
- Yang, H. and Ghose, S. (1994) In situ Fe-Mg order-disorder studies and thermodynamic properties of orthopyroxenes (Fe, Mg)<sub>2</sub>Si<sub>2</sub>O<sub>6</sub>. *American Mineralogist*, 79, 633–643.
- Zema, M., Domeneghetti, M.C., Molin, G.M., and Tazzoli, V. (1997) Cooling rates of diogenites: a study of Fe<sup>2+</sup>-Mg ordering in orthopyroxene by X-ray single-crystal diffraction. *Meteoritics and Planetary Science*, 32, 855–862.
- Zema, M., Domeneghetti, M.C., and Tazzoli, V. (1999) Order-disorder kinetics in orthopyroxene with exsolution products. *American Mineralogist*, 84, 1895–1901.
- Zema, M., Tarantino, S.C., Domeneghetti, M.C., and Tazzoli, V. (2003) Ca in orthopyroxene: structural variations and kinetics of the disordering process. *European Journal of Mineralogy*, 15, 373–380.

MANUSCRIPT RECEIVED JULY 22, 2004

MANUSCRIPT ACCEPTED FEBRUARY 26, 2005

MANUSCRIPT HANDLED BY SIMONA QUARTIERI